The Room-Temperature Rydberg-Atom Receiver For Terahertz Wireless Communications

Yayi Lin,[1,2,a)] Zhenyue She,[1,2,a)] Zhiwen Chen,[1,2] Xianzhe Li,[1,2] Caixia Zhang,[1,2] Kaiyu Liao,[1,2,3] Xinding Zhang,[1,2,3,4] Wei Huang,[1,2,3] Hui Yan,[1,2,3] and Shiliang Zhu[1,2]

[1)]*Guangdong Provincial Key Laboratory of Quantum Engineering and Quantum Materials, School of Physics and Telecommunication Engineering, South China Normal University, Guangzhou 510006, China*

[2)]*Guangdong-Hong Kong Joint Laboratory of Quantum Matter, Frontier Research Institute for Physics, South China Normal University, Guangzhou 510006, China*

[3)]*GPETR Center for Quantum Precision Measurement, South China Normal University, Guangzhou 510006, China*

[4)]*SCNU Qingyuan Institute of Science and Technology Innovation Co., Ltd., Qingyuan 511517, China*

(*Electronic mail: slzhu@scnu.edu.cn)

(*Electronic mail: yanhui@scnu.edu.cn)

(*Electronic mail: WeiHuang@m.scnu.edu.cn)

(Dated: 24 May 2022)

Terahertz wireless communications promises to satisfy the future high-capacity demand. However, practical system for terahertz wireless communications faces many challenges. Among them, the communications distance is a crucial problem due to serious propagation loss. Here we demonstrate a 338.7 GHz wireless link based on the cesium Rydberg atoms in a room-temperature vapor cell. The minimum detectable electric field of $132 \pm 13 \mu V/cm$ (9.72 s detection) is realized in our system. With this atomic receiver, the phase-sensitive conversion of amplitude-modulated or frequency-modulated terahertz waves into optical signals is performed to realize the wireless communications with 8-state phase-shift-keying. The experimental results show that the atomic receiver has many advantages due to its quantum properties. Especially, the communications distance has the potential to be over 18 km. Furthermore, the atomic receiver can be used in the terahertz wireless-fiber link to directly convert the wireless signals into optical signals. Our work provide the new path to future terahertz wireless communications.

Since the data traffic requirement in wireless communication networks is increasing exponentially, the spectral band resources will inevitably be extended to terahertz (THz). And integration of THz links into fibre-optic infrastructures seamlessly is crucial important[1–3]. Significant progress has been made to construct the high performance THz wireless communication systems which mainly consist of transmitters and receivers[4–12]. By combining the photonic transmitter and electronic receiver, the high data rate system transmitting data over 20 m at 237.5 GHz was realized[13]. With all electronic devices, the 21 km wireless communication at 140 GHz was demonstrated[14]. Besides, the graphene-based devices[15,16], plasma-based transistors[17,18] and topological photonics are also promising technologies for THz communication[19].

However, the practical applications of THz wireless communication systems still face great challenges. The free space path loss (FSPL) and atmospheric attenuation make the long distance THz wireless communication difficult[20,21]. Moreover, because the THz transmitter power and receiver sensitivity tend to be lower at higher frequency, it's hard to improve the performance of THz wireless communication systems based on the electronic or photonic devices. Another side, the THz-over-fibre architecture using receiver which can directly convert received wireless signals into optical signals is of great importance but technically difficult[22,23].

Recently, the Rydberg atoms have been demonstrated as electromagnetic field sensors with ultrahigh sensitivity and capability of self-calibration[24–29]: the Rydberg-atom sensors have been proved to be excellent quantum receivers for the microwave communications[30–32]. In the THz frequency range, the Rydberg atoms still have large dipole moment making them ideal candidates for THz quantum sensors[33–36]. The ultimate performance of Rydberg-atom receiver is restricted by the quantum limits. This enables the Rydberg-atom receiver to have potential improving the overall performance of the THz wireless system. Furthermore, the atomic receiver can be used in the THz wireless-to-optical link because it's able to directly convert the wireless signals into the optical ones[37].

In this paper, we demonstrate that the Rydberg atoms in a room-temperature cesium (Cs) vapor cell can be an excellent receiver for THz wireless communication. Firstly, we use the electromagnetically induced transparency (EIT) and Autler-Townes splitting (ATS) technique to calibrate the THz electric field strength produced by a 32-times frequency multiplier source. Then we implement the atomic receiver for THz wireless communication. The phase-sensitive conversion of amplitude-modulated or frequency-modulated THz wave into optical signals is used to perform a canonical digital communication with 8-state phase-shift-keying (PSK). Our work demonstrates that the Rydberg-atom receiver has advantages due to its quantum properties for THz wireless communication. Especially, the communication distance has the potential

[a)]Y. Lin and Z. She contributed equally to this work.

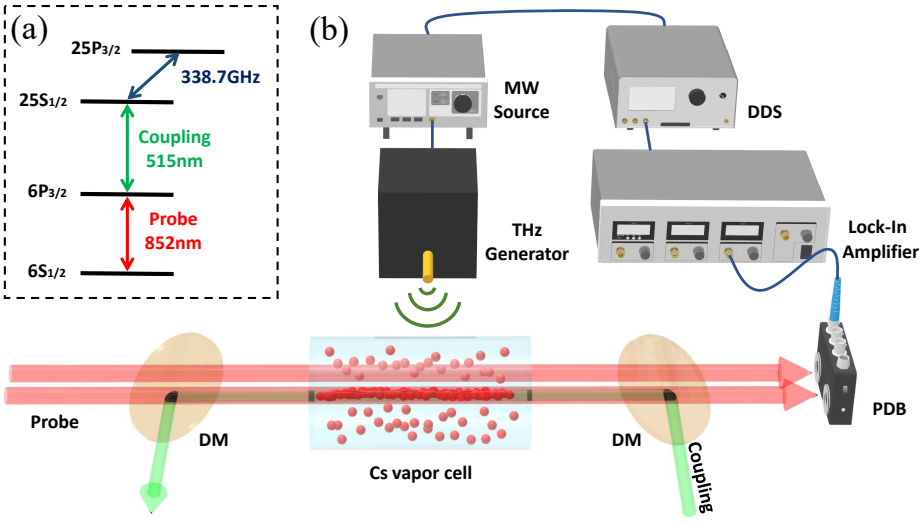

FIG. 1. Level diagram and experimental setup. (a) The four-level system used for the experiments. The probe and coupling light counter-propagate in the vapor cell of cesium atoms. Two dichroic mirrors (DM) are used to combine and split the two beams separately as experiment needed. The terahertz wave couples the Rydberg states $25S_{1/2}$ and $25P_{3/2}$. (b) The experimental setup. The terahertz wave is generated by a 32-times frequency multiplier chain with a commercial microwave source. A two channel direct digital synthesis signal (DDS) generator is used to provide the phase modulated signal for THz wave and reference for lock-in amplifier. An amplified balanced photodetector (PDB) is used to detect the transmission of probe beam. The communication information is demodulated by the lock-in amplifier.

to be over 18 km.

The schematic of the standard four-level EIT-based Rydberg electrometry is illustrated in Fig. 1. The probe and coupling laser beams counter-propagate through a room-temperature Cs vapor cell. The 852 nm probe laser is 100 uW with $1/e^2$ radius 120 μm and the coupling laser is 14.5 mW with $1/e^2$ radius 70 μm. To avoid interfering the probe transmission, both lasers are locked using separated cells by frequency modulation methods. The probe beam is locked to the $6S_{1/2}(F=4) \rightarrow 6P_{3/2}(F'=5)$ transition using the modulation transfer spectroscopy[38]. While the 515 nm coupling laser is locked to the $6P_{3/2} \rightarrow 25S_{1/2}$ transition using the Zeeman modulation scheme[39]. An amplified balanced photodetector (PDB) is served to measure the transmitted probe power subtracting the noisy background to observe EIT. A microwave source (R&S SMF100A) and a 32-times frequency multiplier chain with 26 dBi THz horn provides the 338.7 GHz wave to address the $25S_{1/2} \rightarrow 25P_{3/2}$ Rydberg transition. The THz horn is 15 cm away from the science cell.

The transmission of the probe laser is measured when the coupling laser is scanned. With the THz field on resonance, the EIT peak splits due to the ATS as shown in Fig. 2(a). The AT peak splitting is proportional to the Rabi frequency Ω_{THz} of the THz electric field. With the calculated transition dipole moment $\mu_{THz} = 242ea_0$, the electric field strength $E_{THz} = \hbar\Omega_{THz}/\mu_{THz}$. This relation (linear region) is valid until the splitting is smaller than the linewidth of the EIT peak which is 7.69 MHz in our experiment. To calibrate the minimum detectable THz field, the technique similar to the recently published paper[40]is applied. In the linear region, the measurement of THz electric field is traceable and self-calibrated. The minimal detectable THz electric field in the linear region is $25.37 \pm 0.77\mathrm{mV}/cm$. The electric field strength of THz wave at the atoms is firstly measured in the linear region shown in Fig. 2(b). Then the relationship between THz electric field and fundamental microwave power in the linear region is calibrated shown in Fig. 2(c). Our result shows that the output power of the THz source (32-times frequency multiplier chain) has a nonlinear relationship with the microwave power. To generate the weak THz electric field, the -57.31 dB attenuator is used. After attenuation, the splitting is hard to be distinguished (nonlinear region). The THz detuning is swept to observe the peak of probe transmission (Fig. 2(d)) whose value is positive correlation with THz field strength. From the precisely measured curve of THz electric field versus microwave power, the attenuated field strength can be determined accurately shown in Fig. 2(e). In Fig. 2(f), the variation of THz electric field with microwave power is measured in the nonlinear region. When the signal to noise ratios (SNR) equals 1, the minimum detectable THz electric field is $132 \pm 13\mu V/cm$ (9.72 s detection).

To demonstrate the wireless THz communication using the atomic receiver, the protocol that imposes the modulated THz signal into transmission of probe beam when the the frequencies of laser beams are locked is performed[30]. The digital signal of communication information is encoded in 8 states of modulation phase ϕ_{THz} generated by the digital synthesis signal generator (DDS) in Fig. 1. For frequency modulation, this digital signal is directly sent to the microwave source.

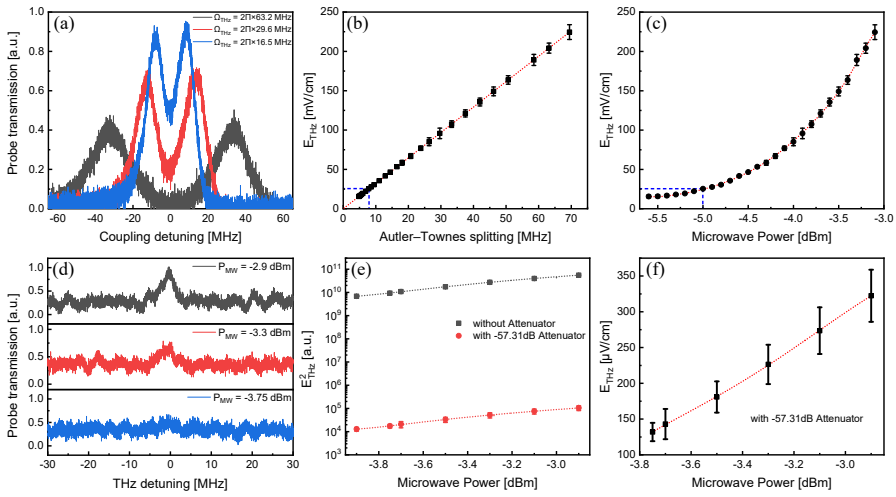

FIG. 2. Characterize the minimum detectable THz electric field. (a) The AT splitting of the $25S_{1/2}$ to $25P_{3/2}$ Rydberg transition that occurs for larger THz electric field with Rabi frequency Ω_{THz}. By scanning coupling laser detuning, the peak splitting of probe transmission corresponds to Ω_{THz}. (b) The linear dependence of THz electric field strength on the AT splitting. The blue dashed line marks where the AT splitting is equal to the EIT linewidth. (c) The THz wave electric field strength versus power of fundamental microwave. (d) The nonlinear region measurement of THz electric field with a minimum value $132 \pm 13 \mu V/cm$ (9.72 s detection). The probe transmission is observed by scanning the THz detuning. (e) The THz electric field in the nonlinear region is obtained precisely. The -57.31dB attenuator is used to reduce the THz eletric field from the accurately measured linear region. (f) The THz wave electric field strength in the nonlinear region versus power of fundamental microwave. The error bars in (b), (c), (e) and (f) indicate standard error from five measurements.

Meanwhile, an external microwave switch controlled by the digital signal is needed to implement the amplitude modulation. Through a 32-times frequency multiplier chain, the modulated THz wave is produced from the microwave. When the THz wave acts on the atoms, the transmission of probe beam is modulated via the EIT process. Thus an amplified balanced photodetector (PDB) is used to monitor the intensity of probe beam after the Cs vapor cell. The communication signal from PDB is analyzed and quadrature demodulated by a lock-in amplifier with reference signal from DDS. After that, the modulated probe transmission by the THz field is demodulated into an In-Phase voltage V_I and a Quadrature-Phase voltage V_Q with the phase $\phi_{de} = \arctan(V_Q/V_I)$. The demodulated phase ϕ_{de} is corresponding to the modulation phase ϕ_{THz} of THz field.

First, the amplitude modulation protocol is tried in the THz wireless communication demonstration. The THz wave is turned on and off by external microwave switch controlled by the phase modulated signal from DDS. In the linear region, the THz electric field is $E_{THz} = 85.18 mV/cm$ and the demodulated 8PSK constellation diagrams is shown in Fig. 3(a). In the nonlinear region, the THz electric field is $E_{THz} = 4.05 mV/cm$ and the demodulated 8PSK constellation diagrams is shown in Fig. 3(b). The 8 phase states are encoded from $\phi_m = 0^\circ$ to $\phi_m = 315^\circ$ with interval 45°. And the modulation frequency 500 kHz and 1 MHz is employed which is limited by the bandwidth of our PDB and lock-in amplifier. Both in the linear region and nonlinear region, the 8 phase states can be clearly discriminated. But the phase noise becomes lager in the nonlinear region since the THz field is weaker.

It's well known that frequency modulation can avoid the influence of amplitude interference in the propagation progress that can significantly improve the communication quality. Therefore, the frequency-modulated methods are also tried in our THz wireless communication scheme. In the frequency modulated communication, the fundamental microwave frequency hopping is controlled by the phase modulated signal from DDS. After 32-times frequency multiplication, detuning of THz wave hops from resonance to a large detuning 156.8 MHz. Relatively, transmission of probe beam varies from maximum peak to small value or even zero when the THz detuning jumps from resonance to 156.8 MHz. So the periodic frequency hopping can be converted into the intensity oscillation of probe beam passing through the Cs vapor cell. Then the collected signal of probe beam intensity by the PDB is sent to the lock-in amplifier. After quadrature demodulation, the 8PSK constellation diagrams illustrated in Fig. 3(c)(d) can be acquired. From Fig. 3, the atomic receiver has the same performance compared with amplitude modulation.

The THz transmission distance is one of the biggest challenges for wireless communication as the serious propagation attenuation. For distance below 1 km, the free space path loss (FSPL) is dominated. The FSPL can be given in terms of the frequency as[41],

$$\mathrm{FSPL} = (4\pi \mathrm{df/c})^2. \quad (1)$$

In our system, the frequency $f = 338.7\ GHz$. Considering the distance $d = 1\ km$ and vacuum speed of light c, the FSPL is 143 dB. For distance large than 1 km, the atmospheric attenuation must be taken into account especially for THz wireless links with large carrier frequency. For example, the atmospheric attenuation is 5 dB/km at 338.7 GHz[9]. One way

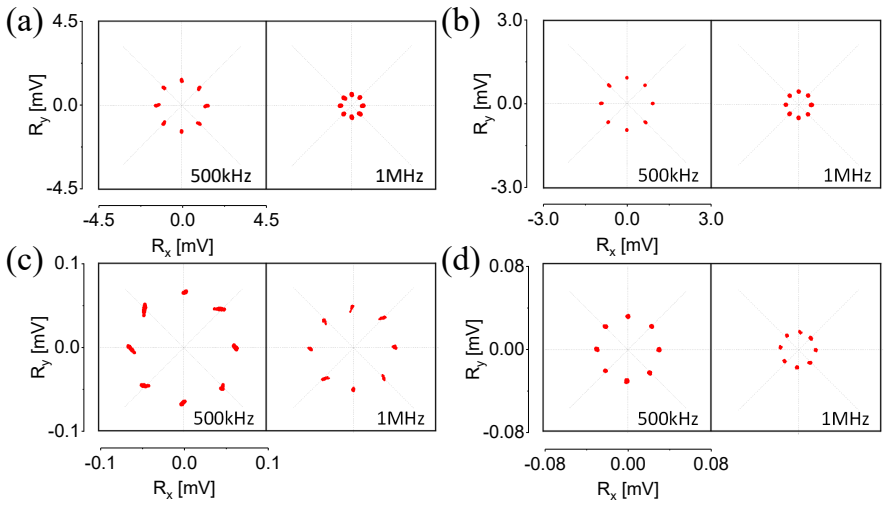

FIG. 3. The demodulated 8PSK diagrams of amplitude-modulated (AM) and frequency-modulated (FM) THz communication. To demonstrate the wireless THz digital communication using the atomic receiver, the protocols that impose the amplitude-modulated and frequency-modulated THz signals into transmission of probe beam are performed. The signals from PDB are analyzed and quadrature demodulated by a lock-in amplifier to obtain the 8PSK diagrams. The THz electric field is $E_{THz} = 85.18 mV/cm$ in the linear region and $E_{THz} = 4.05 mV/cm$ in the nonlinear region. (a) Amplitude modulation with THz electric field in the linear region. The amplitude of demodulation signal decreases when the modulation frequency becomes larger. (b) Amplitude modulation with THz electric field in the nonlinear region. (c) Frequency modulation with THz electric field in the linear region. (d) Frequency modulation with THz electric field in the nonlinear region.

to extend the communication distance is to raise the power of THz source. However, this is very difficult for both photonic and electronic based THz source. Another way is to use the THz receiver with higher sensitivity, that's why we tried the Rydberg-atom receiver. In our THz wireless link, the output power of THz source corresponding to the minimum detectable THz electric field in the nonlinear region is -56 dBm. The full power of the commercial source we used can be 12 dBm, so there is link budget 68 dB for propagation loss. The maximum transmission distance 3.5 m can be achieved. Unlike the electronic receivers, the ultimate sensitivity of the atomic receiver is restricted by the standard quantum limit (SQL). The sensitivity for SQL is described as[42],

$$\frac{E_{\min}}{\sqrt{Hz}} = \frac{2\pi\hbar}{\mu_{THz}\sqrt{NT_2}}. \quad (2)$$

In our experiment, the atom number participating in the EIT progress is $N = 1 \times 10^5$. Considering dephasing time $T_2 = 21\mu s$, the SQL sensitivity is about 2.3 $nVcm^{-1}Hz^{-1/2}$. For room-temperature atoms, the effectiveness of EIT probing is reduced by 30-40 dB[43]. This means the total budget relative to the SQL for wireless transmission is 159-169 dB. Then corresponding distance is about 5 km. Recently, some excellent work has been carried out on embedding the Rydberg-atom sensor into antennas or waveguides[44,45]. If use a 50 dBi transmitter antenna and embedding the Rydberg-atom sensor into a 50 dBi receiver antenna, this distance will be over 18 km. In addition, the Rydberg transitions have large dipole moments in a wide frequency range from 100 GHz to nearly 3 THz, so the atomic receiver can keep this performance in a very wide band[33,36]. Unlike the bandwidth of electronic receiver which is limited by the antennas and waveguides, atomic receiver bandwidth depends on the Rydberg transitions and lasers.

For any type of communication receiver, the maximum channel capacity C is important and described by the Shannon-Hartley Theorem[30,46],

$$C = f_m log_2(1 + SNR). \quad (3)$$

Here the f_m is the symbol frequency and the SNR is signal-to-noise ratio. The modulation frequency is limited by the time needed for the EIT/AT to develop[30,32,46]. Considering maximum 10 MHz modulation frequency, the channel capacity is 10 $Mbits/s$ at the minimum detectable THz field.

Finally, the atomic receiver can be used in the THz wireless-to-optical link because it's able to directly convert the wireless signals into the optical ones[37]. Usually the wireless-to-optical receiver systems rely on electronic devices. The signal of electromagnetic wave is received and mixed down to lower frequency. Then an electro-optic modulator can be used to convert this signal into optical domain[22,23]. In the demonstration of our THz wireless communication system, the amplitude-modulated or frequency-modulated information is directly converted into laser signal at 852 nm by the Rydberg-atom receiver. Comparing with electronic ones, the wireless-to-optical atomic receiver is simpler and lower in cost without frequency down-mixing and extra modulator.

To summarize, the room temperature cesium Rydberg atoms are demonstrated to be sensitive THz electric field sensors. The minimal detectable THz electric fields $132 \pm 13\mu V/cm$ (9.72 s detection) are calibrated. Furthermore, the phase-sensitive conversion of amplitude-modulated and

frequency-modulated THz wave into optical signals is conducted to realize the communication with 8-state phase-shift-keying. The atomic receiver has potential to realize 18 *km* terahertz wireless communication at 338.7 GHz. Furthermore, the atomic receiver can be used in the terahertz wireless-fiber link to directly convert the wireless signals into optical signals. Our work provide the new path to future THz wireless communication.

The work was supported by the Key-Area Research and Development Program of GuangDong Province (Grants No. 2019B030330001 and No. 2020B0301030008), the National Natural Science Foundation of China (Grants No. 61875060, and No. U20A2074), the Key Project of Science and Technology of Guangzhou (Grant No. 2019050001), and the Natural Science Foundation of Guangdong Province (Grants No.2018A030313342).

[1]Seeds, A. J. et al. Terahertz photonics for wireless communications. *J. Lightwave Technol.* **33**, 579-587 (2015).

[2]Yu, X. et al. 160 Gbit/s photonics wireless transmission in the 300¨C500 GHz band. *APL Photon.* **1**, 081301 (2016).

[3]Wang, S. et al. 26.8-m THz wireless transmission of probabilistic shaping 16-QAM-OFDM signals. *APL Photon.* **5**, 056105 (2020).

[4]Kürner, T. & Priebe, S. Towards THz communications ¡a status in research, standardization and regulation. *J. Infrared Milli. Terahz Waves* **35**, 53-62 (2014).

[5]Liu, T.A., Lin, G.R., Chang, Y.C. & Pan, C.L. Wireless audio and burst communication link with directly modulated THz photocondctive antenna. *Opt. Express* **13**, 10416-10423 (2005).

[6]Shams, H. et al. Photonic generation for multichannel THz wireless communication. *Opt. Express* **22**, 23465-123472 (2014).

[7]Nagatsuma, T. et al. Terahertz wireless communications based on photonics technologies. *Opt. Express* **21**, 477-487 (2013).

[8]Li, X. et al. A 400G optical wireless integration delivery system. *Opt. Express* **21**, 187894-187899 (2013).

[9]Nagatsuma, T., Ducournau, G. & Renaud, C. Advances in terahertz communications accelerated by photonics. *Nat. Photon.* **10**, 371-379 (2016).

[10]Harter, T. et al. Generalized Kramers¨CKronig receiver for coherent terahertz communications. *Nat. Photon.* **14**, 601-606 (2020).

[11]Harter, T. et al. Wireless THz link with optoelectronic transmitter and receiver. *Optica* **6**, 001063 (2019).

[12]Wang, C. et al. 0.34-THz Wireless Link Based on High-Order Modulation for Future Wireless Local Area Network Applications. *IEEE Trans. Terahz Sci. Technol.* **4**, 75-85 (2014).

[13]Koenig, S., Lopez-Diaz, D., Antes, J., et al. Wireless sub-THz communication system with high data rate. *Nat. Photon.* **7**, 977-981 (2013).

[14]Wu Q., et al. A 21 km 5 Gbps real time wireless communication system at 0.14 THz. *In 42nd Intl. Conf. on IRMMW-THz*(IEEE, 2017).

[15]Tong, J. Y., Muthee, M., Chen, S. Y., Yngvesson, S. K. & Yan, J. Antenna enhanced graphene THz emitter and detector. *Nano Lett.* **15**, 5295-5301 (2015).

[16]Liu, P. Q. et al. Highly tunable hybrid metamaterials employing split-ring resonators strongly coupled to graphene surface plasmons. *Nature Commun.* **6**, 8969 (2015).

[17]Otsuji, T. Trends in the research of modern terahertz detectors: plasmon detectors. *IEEE Trans. Terahz Sci. Technol.* **5**, 1110-1120 (2015).

[18]Tohme, L. et al. Terahertz wireless communication using GaAs transistors as detectors. *Electron. Lett.* **50**, 323-325 (2014).

[19]Yang, Y., Yamagami, Y. et al. Terahertz topological photonics for on-chip communication. *Nat. Photon.* **14**, 446-451 (2020).

[20]Han, C. et al. Distance-Aware Bandwidth-Adaptive Resource Allocation for Wireless Systems in the Terahertz Band. *IEEE Trans. Terahz Sci. Technol.* **6**, 541-553 (2016).

[21]Han, C. et al. Multi-Ray Channel Modeling and Wideband Characterization for Wireless Communications in the Terahertz Band. *IEEE Trans. Wirel. Commun.* **5**, 1110-1120 (2015).

[22]Salamin, Y. et al. Microwave plasmonic mixer in a transparent fibre¨Cwireless link. *Nat. Photon.* **12**, 749-753 (2018).

[23]Ummethala, S. et al. THz-to-optical conversion in wireless communications using an ultra-broadband plasmonic modulator. *Nat. Photon.* **13**, 519-524 (2019).

[24]Sedlacek, J.A., Schwettmann, A., et al. Microwave electrometry with Rydberg atoms in a vapour cell using bright atomic resonances. *Nature Phys.* **8**, 819-824 (2012).

[25]Holloway, C. L. , Simons, M. T. , Gordon, J. A. , et al. Electric field metrology for SI traceability: Systematic measurement uncertainties in electromagnetically induced transparency in atomic vapor. *J. Appl. Phys.* **121**, 233106 (2017).

[26]Jing, M., Hu, Y., et al. Atomic superheterodyne receiver based on microwave-dressed Rydberg spectroscopy. *Nature Phys.* **16**, 911-915 (2020)

[27]Liao, K. Y. et al. Microwave electrometry via electromagnetically induced absorption in cold Rydberg atoms. *Phys. Rev. A* **101**, 053432 (2020).

[28]Chen, Z. W. et al. Terahertz measurement based on Rydberg atomic antenna. *Acta Phys. Sin.* **70**, 060702 (2021).

[29]Huang, W. et al. Rydberg-atom-based electrometry. *Acta Phys. Sin.* **64**, 160702 (2015).

[30]Meyer, D. H., Cox, K. C.,Fatemi, F. K. & Kunz, P. D. Digital communication with Rydberg atoms and amplitude-modulated microwave fields. *Appl. Phys. Lett.* **112**, 211108 (2018).

[31]Song, Z., Liu, H. Rydberg-atom-based digital communication using a continuously tunable radio-frequency carrier. *Opt. Express* **27**, 8848 (2019).

[32]Simons M. T., et al. A rydberg atom-based mixer: Measuring the phase of a radio frequency wave. *Appl. Phys. Lett.* **114**, 114101 (2019).

[33]Wade, C. G. et al. Real-time near-field terahertz imaging with atomic optical fluorescence. *Nat. Photon.* **11**, 40-43 (2017).

[34]Downes, L. A. et al. Full-Field Terahertz Imaging at Kilohertz Frame Rates Using Atomic Vapor. *Phys. Rev. X* **10**, 011027 (2020).

[35]Wade, C.G. et al. A terahertz-driven non-equilibrium phase transition in a room temperature atomic vapour. *Nature Commun.* **9**, 3567 (2018).

[36]Meyer, D. H. et al. Assessment of rydberg atoms for wideband electrric field sensing. *J. Phys. B: At. Mol. Opt. Phys.* **53**, 034001 (2020).

[37]Deb,A. B. & Kjrgaard, Radio-over-fiber using an optical antenna based on Rydberg states of atoms. *Appl. Phys. Lett.* **112**, 211106 (2018).

[38]Preuschoff, T., et al. Optimization strategies for modulation transfer spectroscopy applied to laser stabilization. *Opt. Express* **26** 24011 (2018).

[39]Jia, F., Zhang J., Zhang L., et al. Frequency Stabilization Method for Transition to Rydberg State using Zeeman Modulation. *Applied Optics* **59** 2108 (2020).

[40]Chen, S, et al. Terahertz electrometry via infrared spectroscopy of atomic vapor. *Optica* **9**, 485-491 (2022).

[41]Pozar, D. M. Microwave Engineering 4th edn (John Wiley and Sons, 2011).

[42]Fan, H.,et al. Atom based RF electric field sensing. *J. Phys. B: At. Mol. Opt. Phys.* **48** 202001 (2015).

[43]Meyer D. H., et al. Optimal atomic quantum sensing using electromagnetically-induced-transparency readout. *Phys. Rev. A* **104**, 043103 (2021).

[44]Simons M.T., et al. Embedding a Rydberg Atom-Based Sensor Into an Antenna for Phase and Amplitude Detection of Radio-Frequency Fields and Modulated Signals. *IEEE Access* **7**, 164975 (2019).

[45]Holloway C.L., et al. A quantum-based power standard: Using Rydberg atoms for a SI-traceable radio-frequency power measurement technique in rectangular waveguides. *Appl. Phys. Lett.* **113**, 094101 (2018).

[46]Cox, K. C., Meyer, D. H., Fatemi, F. K., et al. Quantum-Limited Atomic Receiver in the Electrically Small Regime. *Phys. Rev. Lett.* **121**, 110502.1-110502.6 (2018).